

Intra pseudogap- and superconductivity-pair spin and charge fluctuations and underdome metal-insulator (fermion-boson)-crossover phenomena as keystones of cuprate physics

B. Abdullaev¹, D. B. Abdullaev¹, C.-H. Park², M. M. Musakhanov³

¹Institute of Applied Physics, National University of Uzbekistan, Tashkent 100174, Uzbekistan

²Research Center for Dielectric and Advanced Matter Physics, Department of Physics, Pusan National University, 30 Jangjeon-dong, Geumjeong-gu, Busan 609-735, Korea

³National University of Uzbekistan, Tashkent 100174, Uzbekistan
bakhodir.abdullaev@yandex.ru, cpark@pusan.ac.kr, yousufmm@list.ru

PACS 74.72.-h, 74.20.Mn, 74.25.Fy, 74.25.Bt, 74.25.Jb, 74.25.Ha

DOI 10.17586/2220-8054-2015-6-6-803-824

The most intriguing observation of cuprate experiments is most likely the metal-insulator-crossover (MIC), seen in the underdome region of the temperature-doping phase diagram for copper-oxides under a strong magnetic field, when superconductivity is suppressed. This MIC, which results in such phenomena as heat conductivity downturn, anomalous Lorentz ratio, nonlinear entropy, insulating ground state, nematicity- and stripe-phases and Fermi pockets, reveals the nonconventional dielectric property of the pseudogap-normal phase. Since conventional superconductivity appears from a conducting normal phase, the understanding of how superconductivity arises from an insulating state becomes a fundamental problem and thus the keystone for all of cuprate physics. Recently, in interpreting the physics of visualization in scanning tunneling microscopy (STM) real space nanoregions (NRs), which exhibit an energy gap, we have succeeded in understanding that the minimum size for these NRs provides pseudogap and superconductivity pairs, which are single bosons. In this work, we discuss the intra-particle magnetic spin and charge fluctuations of these bosons, observed recently in hidden magnetic order and STM experiments. We find that all the mentioned MIC phenomena can be obtained in the Coulomb single boson and single fermion two liquid model, which we recently developed, and the MIC is a crossover of sample percolating NRs of single fermions into those of single bosons.

Keywords: high critical temperature superconductivity, cuprate, metal-insulator-crossover, temperature-doping phase diagram, heat conductivity downturn, anomalous Lorentz ratio, nonlinear entropy, insulating ground state, stripe phase, Fermi pocket.

Received: 1 November 2015

1. Introduction

The origin of pseudogap (PG) and high-temperature superconductivity (HTS) phases in copper oxides (cuprates) is one of the most puzzling and challenging problem in condensed matter physics. Despite being almost three decades since their discovery, intensive experimental and theoretical studies have yielded little clear understanding of these phases so far. The experimental studies of HTS and PG in cuprates have provided physicists with numerous interesting and fascinating materials with unconventional properties. Among the

most puzzling and thus far most intriguing is the observation of the metal-insulator-crossover (MIC), seen in the underdome region of a temperature-doping phase diagram in the presence or absence of a strong external magnetic field [1,2]. The MIC, detected after suppression of the HTS by a strong magnetic field, results in a number of different phenomena: heat conductivity downturn and anomalous Lorentz ratio [3,4], nonlinear entropy [5,6], insulating ground state [1,2], dynamic nematicity [7] and static stripe phases [8] and Fermi pockets [8,9]. This reveals the highly unconventional dielectric property of the PG-normal phase of these superconductors. Since superconductivity appears in conventional superconductors from the conducting normal state only, the understanding of how HTS arises from an insulating state becomes a fundamental problem, and thus, the keystone for cuprate physics. This MIC also separates previously applied mechanisms and models for conventional superconductors from the consideration. However, the answer to the question “What quasiparticles do provide the PG and HTS phases?” still remains elusive.

In Ref. [10], we demonstrated that these quasiparticles are PG and HTS pairs. We came to this conclusion when trying to interpret the physics visualized in STM real space PG and HTS nanoregions [11,12], which exhibited an energy gap. In [10], we showed that the minimal size of these nanoregions are real space pairs and furthermore, these pairs are single bosons. We also have a good qualitative understanding of all elements for the temperature-doping phase diagram for copper-oxides. We have shown that the precursor mechanism for HTS is valid, when bulk superconductivity at the critical temperature T_c or at the first critical doping x_{c1} appears as a percolation phase transition for the spatial overlapping of separated PG pairs.

In this work, we discuss the intra particle spin and charge fluctuations of PG and HTS pairs - single bosons, observed recently in hidden magnetic order [13] and STM [14] experiments. We find that all the above-mentioned MIC phenomena might be obtained in the framework of the Coulomb single boson and single fermion two liquid model [10], which naturally emerges from the analysis of the STM experimental data [11,12] and thus draw a conclusion about the single boson nature of the visualized in the STM experimental pairs.

Currently, we realize that the non-Fermi liquid property of these phenomena and thus of copper oxides is related to the mutual single boson and MIC physics. The insulating ground state of cuprates is a result of a gas composed of single bosons. According to the Bogoliubov approach for gas of charged bosons [15], at high gas density, where this approach is valid, the ground state energy consists of components for the Bose-Einstein condensate and a gas of quasi-particles. At high magnetic fields or at lower levels with doping, to the first critical level, for which all MIC phenomena are measured, the Bose-Einstein condensate vanishes and there, only a gas of quasi-particles exists, i.e., a gas of 2D plasmons of singly-charged bosons. However, the latter is insulating, therefore, the insulator is the whole ground state of copper oxides for underdome dopings from the first critical level (x_{c1}) up to the second critical level (x_{c2}). It is worth noting here that typically, the experiment detects the MIC up to the critical value of doping x_c , which, for some cuprates, coincides with the optimal doping, at which the T_c is maximum in the temperature-doping phase diagrams, and for others, with the second critical doping level x_{c2} . For the sake of simplicity, we assume that x_c coincides with x_{c2} .

According to the phenomenological Coulomb single boson and single fermion two liquid model, fermions, which are responsible for the electrical conductivity, emerge in the system at the first critical doping level x_{c1} . They are not active in the sense of contributing to the bulk electrical conductivity in the range between x_{c1} and x_{c2} . Only from the second critical doping level x_{c2} , beyond which the spatial percolation of NRs for fermions occurs,

do these fermions contribute to penetration of charges in entire volume of a sample. From this analysis, we realize that the MIC is the fermion - boson crossover of sample percolating NRs of single fermions into that of single bosons. As it was shown below (see also Ref. [10]), NRs of single fermions start to percolate from x_{c2} while those of single bosons do so from x_{c1} .

The insulating behavior of fermions in the normal phase underdome region of doping results in the insulating property of Fermi pockets, which is a generalization of the insulating Fermi pockets, seen in angle resolved photoemission spectroscopy (ARPES) experiment [9] (for details see Sec. 9). The observed underdome doping evolution of these pockets qualitatively coincides with that of a gas of fermions in the Coulomb two liquid model. These insulating fermions also result in an insulating stripe phase (the smectic phase), seen in the PG phase of some copper oxides [8], when fermion charges, with their collective static electric field, deform the parent compound lattice, consisting of electrically polar atoms.

It is interesting that the spatially intra rare charge density of each single boson (see the size of last one in the table of Sec. 6) allows one to understand the nature of the intra-unit cell nematic order (the dynamic charge fluctuations) for the sample hole density and its evolution with doping, which was recently observed in the STM experiment [14]. This is also the result of the strong ferrielectric crystal field of the parent compound and the decrease of single bosons with doping.

The interesting hidden magnetic order experiment [13] has revealed the existence of objects in the PG phase with zero total spin but with its fluctuations inside. Despite the authors' (Ref. [13]) interpretation of the physical meaning of both spins, by suggesting either a pair of oppositely flowing intra-structural cell loop-currents or staggered spins in the same cell, the role of these objects in cuprate physics was not understood. One could assume that these objects are the PG and HTS pairs (for justification of this assumption see Sec. 7 below), however, the two mentioned mechanisms for explaining the object's spins were unable to provide the large experimental value for the pair energy gap which was observed for cuprates. This shortcoming was improved upon in our research [16, 17], which appeared in publication in the same year as the experiment described in [13] and reproduced the experimental values of the T_c . In these papers, we have succeeded in understanding not only the nature of both object spins, but also predict their evolution with doping. This evolution was successfully observed in further experiments on the hidden magnetic order.

In Sec. 2, we demonstrate the rigorous proof that $2D$ fermions can bosonize. Then, in Sec. 3, the results for the ground-state energy calculations of a charged anyon gas will be given. We apply the difference between the ground state energies of fermions and bosons to derive the single boson doping-temperature phase diagram for cuprates in Sec. 4. In Sec. 5, it will be demonstrated that this difference in the ground state energies yields the microscopic origin of the phenomenological Uemura relation. Sec. 6 will be devoted to the charge and percolation analysis of NRs on the basis of experimental data given in Refs. [11] and [12]. This analysis provides the interpretation for some elements of the phase diagram doping-temperature for $Bi_2Sr_2CaCu_2O_{8+\delta}$. In Sec. 7, we will demonstrate that intra-structural cells, for which the hidden magnetic order has been observed, are NR's, as displayed by the STM experiment [11] and thus single bosons. We also show in this section that intra cell spin fluctuations and an electronic nematicity [14] can naturally be understood within the single boson model. The MIC and insulating ground state, observed in a set of copper oxides, and their possible understanding within the framework of the Coulomb two liquid model is subject of Sec. 8. The origin of Fermi pockets and stripe phases, seen experimentally in some cuprates, is discussed in Sec. 9 for our model. The answer for the interesting question:

“Why is the ground state of YBCO copper oxides in a strong magnetic field an oscillating Fermi Liquid, while for $Bi_2Sr_2CaCu_2O_{8+\delta}$ cuprate, it is insulating?” can be found in the Sec. 10. Sec. 11 will describe the origin of the non-Fermi liquid heat conductivity and the entropy of copper-oxides. We summarize and conclude our paper in Sec. 12.

2. Real Bosonization of 2D Fermions

The 2D topology allows fractional statistics [18], characterized by a continuous parameter ν , having values between 0 (for bosons) and 1 (for fermions). The particles with $0 < \nu < 1$ are generically called anyons [19]. One can apply the last criterion to investigate the properties of the $a - b$ planes of CuO_2 atoms, which play a dominant role in the determination of cuprate physics.

In a manner similar to Ref. [10], we briefly outline the rigorous derivation of the real bosonization of 2D fermions in this section. This can be achieved by exact cancellation of terms in the Hamiltonian arising from fermion (anyon) statistics and a Zeeman interaction of spins $\hbar/2$ of particles with statistical magnetic field [20] produced by vector potential of anyons.

Let us consider the Hamiltonian

$$\hat{H} = \frac{1}{2M} \sum_{k=1}^N \left[\left(\vec{p}_k + \vec{A}_\nu(\vec{r}_k) \right)^2 + M^2 \omega_0^2 |\vec{r}_k|^2 \right] + \frac{1}{2} \sum_{k=1}^N \left[V(\vec{r}_k) + \sum_{j \neq k}^N \frac{e^2}{|\vec{r}_{kj}|} \right] \quad (1)$$

of the gas of N anyons with mass M and charge e , confined in a 2D parabolic well, interacting through Coulomb repulsion potential in the presence of a uniform positive background [21] $V(\vec{r}_k)$. Here, \vec{r}_k and \vec{p}_k represent the position and momentum operators of the k th anyon in 2D space dimension,

$$\vec{A}_\nu(\vec{r}_k) = \hbar\nu \sum_{j \neq k}^N \frac{\vec{e}_z \times \vec{r}_{kj}}{|\vec{r}_{kj}|^2} \quad (2)$$

is the anyon gauge vector potential [22], $\vec{r}_{kj} = \vec{r}_k - \vec{r}_j$, and \vec{e}_z is the unit vector normal to the 2D plane. In the expression for $\vec{A}_\nu(\vec{r}_k)$ and hereafter, we assume that $0 \leq \nu \leq 1$.

In the bosonic representation of anyons we take the system wave function in the form [23]:

$$\Psi(\vec{R}) = \prod_{i \neq j} r_{ij}^\nu \Psi_T(\vec{R}). \quad (3)$$

Here, $\vec{R} = \{\vec{r}_1, \dots, \vec{r}_N\}$ is the configuration space of the N anyons. The product in the right hand side of this equation is the Jastrow-type wave function. It describes the short distance correlations between two particles due to anyonic (fermionic) statistical interaction.

Let us consider first the term in the Hamiltonian \hat{H} , Eq. (1), containing the anyon vector potential $\vec{A}_\nu(\vec{r}_k)$. Substituting $\Psi(\vec{R})$, Eq. (3), into the Schrödinger equation with this Hamiltonian, we obtain an equation $\hat{H}\Psi_T(\vec{R}) = E\Psi_T(\vec{R})$ with the novel Hamiltonian $\tilde{H} = \tilde{H}_1 + \tilde{H}_2$, where:

$$\tilde{H}_1 = \sum_{k=1}^N \left(\frac{-\hbar^2 \Delta_k}{2M} - \frac{\hbar^2 \nu}{M} \sum_{j \neq k} \frac{\vec{r}_{kj} \cdot \vec{\nabla}_k}{|\vec{r}_{kj}|^2} \right) \quad (4)$$

and

$$\tilde{H}_2 = -i \frac{\hbar}{M} \sum_{k=1}^N \left(\vec{A}_\nu(\vec{r}_k) \cdot \vec{\nabla}_k + \nu \sum_{j \neq k} \frac{\vec{A}_\nu(\vec{r}_k) \cdot \vec{r}_{kj}}{|\vec{r}_{kj}|^2} \right). \quad (5)$$

As shown in Ref. [23], the ν interaction Hamiltonian in \tilde{H}_1 , i.e., the second its term, is equivalent to the sum of the two-body potentials (accuracy of this term discussed in [10])

$$\frac{\pi \hbar^2 \nu}{M} \sum_{j \neq k} \delta^{(2)}(\vec{r}_k - \vec{r}_j). \quad (6)$$

Therefore, the Hamiltonian \tilde{H}_1 now reads

$$\tilde{H}_1 = \sum_{k=1}^N \left(\frac{-\hbar^2 \Delta_k}{2M} + \frac{\pi \hbar^2 \nu}{M} \sum_{j \neq k} \delta^{(2)}(\vec{r}_k - \vec{r}_j) \right). \quad (7)$$

Now, we demonstrate the real bosonization of $2D$ fermions for the example of anyons in a parabolic well. To do this, we consider the Zeeman interaction term:

$$\frac{\hbar}{M} \sum_{k=1}^N \hat{s} \cdot \vec{b}_k \quad (8)$$

of spins with the statistical magnetic field [20]

$$\vec{b}_k = -2\pi \hbar \nu \vec{e}_z \sum_{j \neq k} \delta^{(2)}(\vec{r}_k - \vec{r}_j), \quad (9)$$

which can be derived if one calculates $\vec{b}_k = \vec{\nabla} \times \vec{A}_\nu(\vec{r}_k)$ by using Eq. (2).

For $s_z = \hbar/2$, and using the expression, Eq. (9), one obtains the following for the Zeeman term:

$$\frac{\hbar}{M} \sum_{k=1}^N \hat{s} \cdot \vec{b}_k = -\pi \nu \frac{\hbar^2}{M} \sum_{k(j \neq k)} \delta^{(2)}(\vec{r}_k - \vec{r}_j). \quad (10)$$

It is easy to see that the contribution to the energy from the Hamiltonian \tilde{H}_2 is zero. On the other hand, this expression for the Zeeman term, added to Eq. (7), exactly cancels the second term of \tilde{H}_1 , which is responsible for fermion (for $\nu = 1$) and anyon statistics. Since the energy for bosons is lower than that of fermions and anyons, there appears a coupling of spin with statistical magnetic field for every particle or bosonization of $2D$ fermions and anyons. From this, one can conclude that if anyon concept is correct for the description of any $2D$ quantum system, its ground state should be bosonic with $\nu = 0$, while its excited state should be fermionic ($\nu = 1$) or anyonic ($0 < \nu < 1$), depending upon the fixed value for ν .

3. The ground-state energy of charged anyon gas

In Ref. [15], we derived an approximate analytic formula for the ground-state energy of a charged anyon gas. Our approach was based on the harmonically confined two-dimensional ($2D$) Coulomb anyon gas and a regularization procedure for vanishing confinement. To take into account the fractional statistics and Coulomb interaction, we introduced a function, which depends on both the statistical and density parameters (ν and r_s , respectively). We determined this function by fitting our energy to the ground state energies of the classical electron crystal at very large r_s (the $2D$ Wigner crystal), and to the Hartree-Fock (HF)

energy of the spin-polarized 2D electron gas, and the dense 2D Coulomb-Bose gas for very small r_s . The latter was calculated by use of the Bogoliubov approximation. When applied to the boson system, ($\nu = 0$), our results were very close to those obtained recently from Monte Carlo (MC) calculations. For spin-polarized electron systems ($\nu = 1$), our comparison led to a critical judgment concerning the density range, to which the HF approximation and MC simulations apply.

We have found in Ref. [15] the expression for the ground-state energy per particle (in Ry units) in the form

$$\mathcal{E}_0(\nu, r_s) \approx \frac{2f(\nu, r_s)}{r_s^2} \left[\frac{\nu}{2K_X^2} + \frac{K_X^2}{2} - \frac{K}{K_X} \right]. \quad (11)$$

Here,

$$K_X = (K_A + K_B)^{1/2} + [-(K_A + K_B) + 2(K_A^2 - K_A K_B + K_B^2)^{1/2}]^{1/2}, \quad (12)$$

and

$$\begin{aligned} K_A &= \left[K^2/128 + ((\nu/12)^3 + (K^2/128)^2)^{1/2} \right]^{1/3}, \\ K_B &= \left[K^2/128 - ((\nu/12)^3 + (K^2/128)^2)^{1/2} \right]^{1/3}, \end{aligned} \quad (13)$$

with $K = c_{WC} r_s / f^{1/2}(\nu, r_s)$.

For the Bose gas ($\nu = 0$), we obtained from Eq. (11):

$$\mathcal{E}_0(0, r_s) = -\frac{c_{WC}^{2/3} f^{2/3}(0, r_s)}{r_s^{4/3}}. \quad (14)$$

We found for small r_s that $f(0, r_s) \approx c_{BG}^{3/2} r_s / c_{WC}$, which matched the ground-state energy of Coulomb Bose gas calculated in Ref. [15] using the Bogoliubov approximation with $c_{BG} = 1.29355$. For large r_s , the ground-state energy does not depend on statistics and equals the energy of the classical 2D Wigner crystal [24], $E_{WC} = -2.2122/r_s$. This matches with Eq. (14) if at low densities $f(0, r_s) \approx r_s^{1/2}$ with $c_{WC}^{2/3} = 2.2122$. For large r_s , we obtained:

$$\mathcal{E}_0(\nu, r_s \rightarrow \infty) = \frac{c_{WC}^{2/3} f^{2/3}(\nu, r_s)}{r_s^{4/3}} \left(-1 + \frac{7\nu f^{2/3}(\nu, r_s)}{3c_{WC}^{4/3} r_s^{4/3}} \right). \quad (15)$$

For an arbitrary r_s , the interpolating functional form is:

$$\begin{aligned} f(\nu, r_s) &\approx \nu^{1/2} c_0(r_s) e^{-5r_s} \\ &+ \frac{c_{BG}^{3/2} r_s / c_{WC}}{1 + c_1(r_s) c_{BG}^{3/2} r_s^{1/2} / c_{WC}} + \frac{0.2c_1(r_s) r_s^2 \text{Ln}(r_s)}{1 + r_s^2} \end{aligned} \quad (16)$$

with $c_0(r_s) = 1 + 6.9943r_s + 22.4717r_s^2$ and $c_1(r_s) = 1 - e^{-r_s}$ satisfying all constraints for the $f(\nu, r_s)$ function (see Ref. [15]) and, in addition, yields in the fermion case ($\nu = 1$) for the ground-state energy per particle the following HF result [25]:

$$E_{HF} = \frac{2}{r_s^2} - \frac{16}{3\pi r_s}. \quad (17)$$

In Fig. 1, we show the results for the ground-state energy per particle on the large scale $1.0 \leq r_s \leq 15.0$. The upper four curves refer in descending order to the following fermion cases ($\nu = 1$): HF energies for spin-polarized electrons from Ref. [25] (open triangles); interpolation by Padè approximant MC data from Ref. [26] for spin-polarized electrons (crosses); our results from Eq. (11) (on the given scale identical with those of Eq. (15))(plus

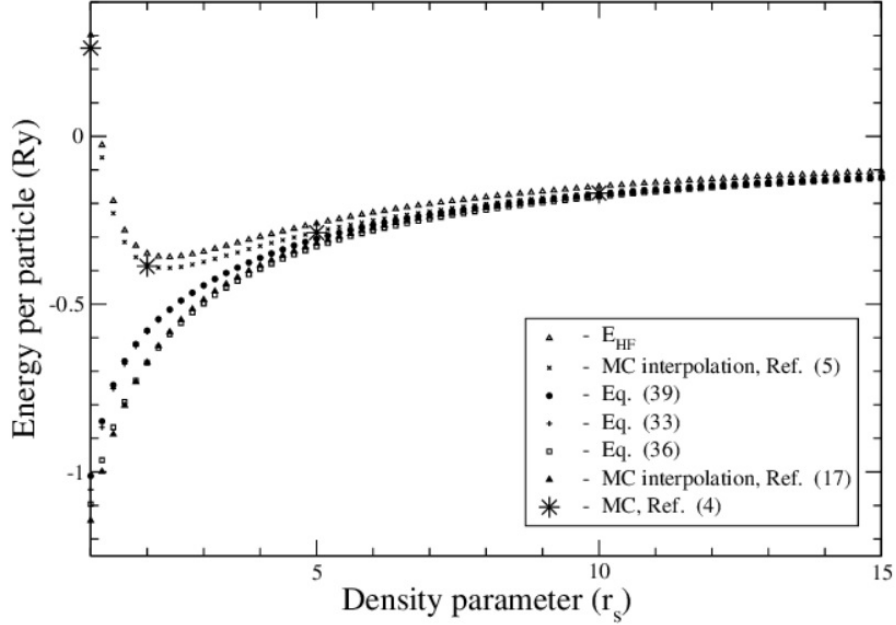


FIG. 1. Ground-state energies per particle vs density parameter r_s values ranging from $1.0 \leq r_s \leq 15.0$ from top to bottom: for fermions ($\nu = 1$) HF approximation (Eq. (17) and Ref. [25], open triangles), MC interpolation data (from Ref. [26] (Ref.[5] in [15])), (crosses), and present results from Eq. (15) (Eq.(39) in [15]) (closed circles) and Eq. (11) (Eq.(33) in [15]) (plus signs), and for bosons ($\nu = 0$) present results from Eq. (14) (Eq.(36) in [15]) (open squares) and MC data from Ref. [27] (Ref.[17] in [15]) (closed triangles). MC data of Ref. [28] (Ref.[4] in [15]) for some particular values of r_s are indicated by star symbols

signs); and our results from Eq. (15) for spin-polarized electrons (closed circles). The lower two curves are for charged bosons ($\nu = 0$) and result from MC calculations of Ref. [27] (closed triangles) and from our Eq. (14) (open squares). By star symbols, we indicated the MC data [28] (without interpolation) obtained for some particular r_s values.

4. Single Boson doping-temperature phase diagram

Following Refs. [16,17], one can assume that coupled to anyon magnetic field spins of fermions are fluctuating. Therefore, bosons with effective spins might appear as Fermi particles. However, fermions with different spins are independent [29]. Thus, the spins of bosons interact with each other and do not interact with spins of another fermions if they exist in the system. We introduce a correlation length, inside of which, spins of bosons interact with each other. For temperature $T = 0$ we denote it by ξ_0 . The increase of fluctuations destroys the coupling, and bosons become the anyons or fermions. This occurs when the gain in the energy due to fluctuations of spins of bosons is equal to energy difference between the anyon (or Fermi) and Bose ground states.

For the interaction of boson spins, we introduce the following form:

$$e^{-r_0/\xi_0} \sum_{k=1}^N \hat{s}_{k+\delta} \cdot \hat{s}_k . \quad (18)$$

Here, a factor e^{-r_0/ξ_0} was introduced with r_0 being the mean distance between particles. For screening by magnetic field spins, ξ_0 is assumed to be phenomenological and taken from the experiment.

We establish the explicit form of Eq. (18). The growth of boson spin fluctuations should cancel term, Eq. (8), in the Hamiltonian. Therefore, for a dense Bose gas ($r_0 < \xi_0$), the following should hold: $\hat{s}_{k+\delta} = -\hbar\vec{b}_k/M$.

The Hamiltonian of a bosonized infinite anyon Coulomb gas with spin interaction has the form:

$$\hat{H} = \frac{1}{2M} \sum_{k=1}^N \left[\left(\vec{p}_k + \vec{A}_\nu(\vec{r}_k) \right)^2 + MV(\vec{r}_k) \right] + \frac{1}{2} \sum_{k,j \neq k}^N \frac{e^2}{|\vec{r}_{kj}|} + \frac{\hbar(1 - e^{-r_0/\xi_0})}{M} \sum_{k=1}^N \hat{s}_k \cdot \vec{b}_k. \quad (19)$$

For an anyon Coulomb gas with density parameter $r_s > 2$, where r_s is r_0 in Bohr radius a_B units, the approximate ground state energy per particle is expressed by Eq. (15). In our treatment we consider the bosonized fermions with $\nu = 1$. To become fermions, bosons should overcome the energy difference:

$$\Delta_0^B = \frac{7(1 - e^{-r_s/\xi_0})f^{4/3}(0, r_s)}{3c_{WC}^{2/3}r_s^{8/3}}, \quad (20)$$

i.e., the superconductivity gap. Our approach in [15] corresponds to spinless or fully spin-polarized fermions. Our system is a normal, i.e., non-spin-polarized electron liquid. However, for intermediate values of r_s , in which we have interest, according to Ceperley MC data [26], there is a tiny difference of ground state energies for spin-polarized and non-spin-polarized electrons. Therefore, we can use ground-state energy for spin-polarized fermions.

The Fig. 2 displays the PG boundary energy E_g (Fig. 11 from paper [30]), superconductivity gap energy $\Delta_0 = 4K_B T_c$, which was evaluated using the empirical formula $T_c = T_{c,max}[1 - 82.6(p - 0.16)^2]$ with $T_{c,max} = 95 K$ for Bi_{-2212} ($Bi_2Sr_2CaCu_2O_{8+\delta}$) compound, and energy gap calculated from Eq. (20) as function of doping p . As seen from this figure, our Δ_0^B has the same magnitude as the experimental gap, but is qualitatively different from the generally accepted ‘‘dome’’ like doping-temperature phase diagram. However, it is in accordance with Fig. 10 of paper [30] of Tallon and Loram and their conclusion that PG energy E_g up to $p_c \approx 0.19$ separates the Bose-Einstein condensate into regions, where the densities of Cooper pairs are small and large (weak and strong superconductivity).

For the phase diagram data of electron-doped cuprates, we use Ref. [31] for NCCO ($Nd_{2-x}Ce_xCuO_4$) and Ref. [32] for PCCO ($Pr_{2-x}Ce_xCuO_4$). It was shown there that $E_g/(k_B T^*) \approx 10$ for NCCO and $E_g/(k_B T^*) \approx 11$ for PCCO, therefore, we assume $E_g/(k_B T^*) \approx 10$ for both materials. For the experimental superconductivity gap, we also assume $\Delta_0/(k_B T_c) \approx 10$. Fig. 3 shows the doping p dependence of experimental E_g , $\Delta_0 = 10k_B T_c$ and Δ_0^B calculated from Eq. (20) by using the above spacing constants of a and b for an elementary structural cell. Comparing with Fig. 2, we see similar qualitative and quantitative results. More obvious is the extension of our Δ_0^B to small values of p , while experimental Δ_0 starts with $p = 0.13$. However, the absolute values for both superconductivity gaps of hole- and electron-doped materials are nearly equal.

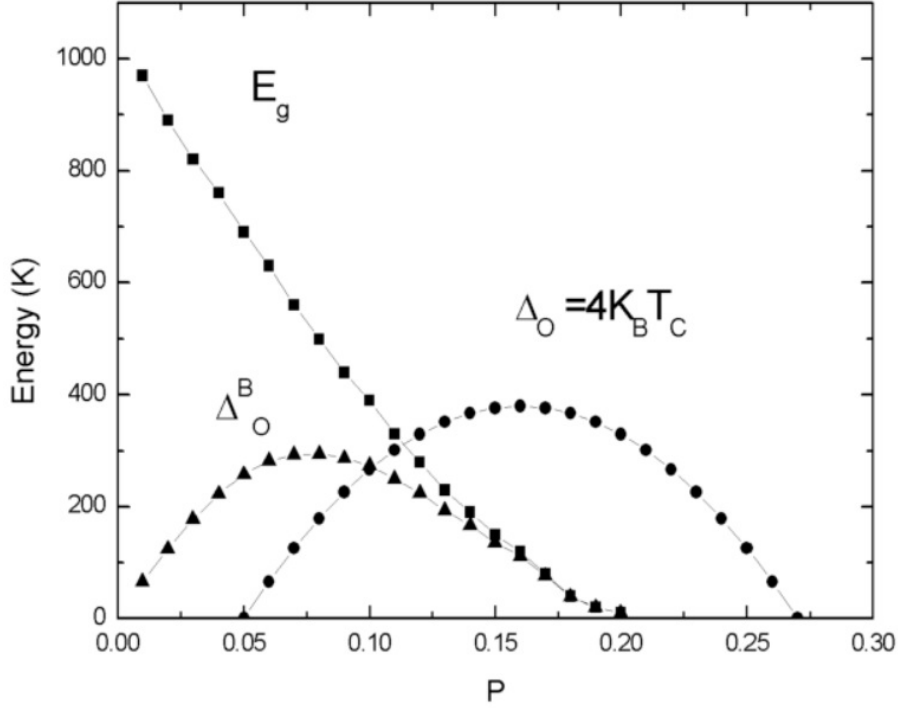


FIG. 2. The experimental PG E_g , superconductivity gap $\Delta_0 = 4K_B T_c$ (experiment for hole-doped *Bi* - 2212 compound), and calculated from formula Eq. (20) one for bosons Δ_0^B energies in Kelvin temperature (K) units as function of concentration of holes p

5. Origin of Uemura Relation

In this section, following Ref. [10], we describe the single boson origin of the phenomenological Uemura relation for $2D$ superconductors.

Currently, it is widely accepted (see Ref. [33]) that the Uemura relation (UR), i.e. the linear dependence of T_c on the concentration of the charge carriers, originally observed in Refs. [34] and [35] for under-doped cuprate, bismuthate, organic, Chevrel-phase and heavy-fermion superconductors, also survives for the extended class of other superconductors and has a fundamentally universal character. An experiment clearly relates the UR with $2D$ geometry of samples. Motivated by this observation, in Ref. [10], we investigated the possible role of the fermion bosonization, which is a result of the topology of $2D$, to the origin of UR.

The experimental doping dependence of r_0 mean distance between two holes, can be approximated by the relationship $r_0 \approx a/x^{1/2}$ (see Fig. 34 in Ref. [36]), where a is the lattice constant in an elementary structural plaquette for the CuO_2 $a-b$ plane of a copper oxide. Since, in [10], the doping value is denoted by the variable x , we keep this notation in this and another section below, which are written on the basis of Ref. [10]. This relationship is derived in Ref. [36] for $La_{2-x}Sr_xCuO_4$ with $a \approx 3.8\text{\AA}$. This lattice constant a is the nearly identical to the other copper oxide compounds, thus it is also valid for investigating $Bi_2Sr_2CaCu_2O_{8+\delta}$. It is worth noting that $b \approx a$ for the lattice constant b for the same structural plaquette.

Applying the relationship $r_0 \approx a/x^{1/2}$, where $a \approx 3.8\text{\AA}$, we estimate the values of r_0 , expressed in Bohr radius a_B unit ($r_s = r_0/a_B$), corresponding to the doping interval

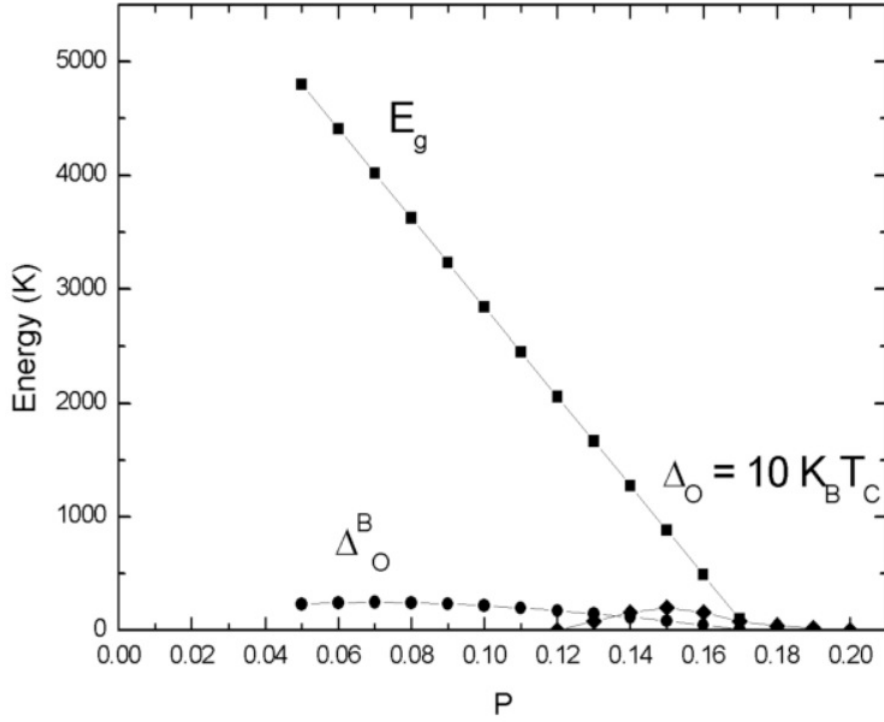


FIG. 3. The experimental PG E_g , superconductivity gap $\Delta_0 = 10K_B T_c$ (experiments for electron-doped NCCO and PCCO compounds), and value calculated from formula Eq. (20) for bosons energies Δ_0^B in Kelvin temperature (K) units as a function of electron concentration, p

$x_{c1} \leq x \leq x_{c2}$, where x_{c1} and x_{c2} are the first and second critical dopings in the doping-temperature phase diagram. When doing so, one sees that $13.12 \leq r_s \leq 32.14$. For this interval of r_s , we obtained the expression, Eq. (15), for the ground state energy per particle of the Coulomb-interacting anyon gas. It is expressed in Ry (Rydberg) energy units, and for large r_s , equals the energy of the classical 2D Wigner crystal [24], $E_{WC} = -c_{WC}^{2/3}/r_s$ with $c_{WC}^{2/3} = 2.2122$.

Taking into account from the previous section that the excited state of the 2D system is fermionic and the ground state is bosonic, one can write the explicit expression for an energy gap between these two states in the following manner:

$$\Delta(r_s) = \mathcal{E}(\nu = 1, r_s) - \mathcal{E}(\nu = 0, r_s) = \frac{7E_{WC}^2}{3c_{WC}^2}. \quad (21)$$

The meaning of this expression is that to become a fermion, the boson should gain the energy $\Delta(r_s)$. Substituting in Eq. (21) the expression for E_{WC} , and introducing the 2D density, $n = 1/(\pi r_0^2)$, one derives:

$$\Delta(n) = \frac{7\pi n a_B^2}{3c_{WC}^{2/3}}. \quad (22)$$

Since the critical temperature T_c is proportional to $\Delta(n)$, one can conclude that the 2D topology driven bosonization of fermions may explain the UR for a variety superconductors, whose physics is quasi - two dimensional.

6. Experiment implied single boson elements of the doping-temperature phase diagram

Recently, Gomes *et al.* [11] have visualized the gap formation in NRs above the critical temperature T_c in the HTS $Bi_2Sr_2CaCu_2O_{8+\delta}$ cuprate. It has been found that, as the temperature lowers, the NRs expanded in the bulk superconducting state consisted of inhomogeneities. The fact that the size of the inhomogeneity [12] is close to the minimum size of the NR [11] leads to a conclusion that the HTS phase is a result of these overlapped NRs. In the present section, we reproduce the main results of Ref. [10], where the charge and percolation regime analysis of NRs was performed and shown that at the first critical doping x_{c1} , when the superconductivity initiates, each NR carries a positive electric charge of one (in units of electron charge), thus we attributed the NR to a single hole boson, and the percolation lines connecting these bosons emerged. At the second critical doping x_{c2} , when superconductivity disappears, our analysis demonstrated that the charge of each NR equals two. The origin of x_{c2} can be understood by introducing additional normal phase hole fermions in NRs, whose concentration appearing above x_{c1} increases smoothly with doping and breaks the boson percolation lines at x_{c2} . The latter resulted in the disappearance of the bulk bosonic properties of the PG region, which explained the upper bound for the existence of vortices in the Nernst effect [37]. Since [11] demonstrated the absence of NRs at the PG boundary, one can conclude that along this boundary, as well as in x_{c2} , all bosons disappear.

The authors of Ref. [11] have visualized the NRs in the PG region of $Bi_2Sr_2CaCu_2O_{8+\delta}$ at fixed hole dopings of $x = 0.12, 0.14, 0.16, 0.19, 0.22$. It has been determined that for $x = 0.16$ and $x = 0.22$, the minimum size of the NRs is $\xi_{coh} \approx 1 - 3$ nm. The estimated minimum size of NRs, ξ_{coh} , is 1.3 nm in the superconducting phase [12] ($T_c = 84K$). Another notable result obtained in Ref. [12] was the observation of spatial localization for the doped charges. The charges were localized in the same area as NRs [12] with the same coherence length ξ_{coh} .

The principal part of our analysis in Ref. [10] has been the doping x dependence of the NR charge $(\xi_{coh}/r_0)^2$. We started with the case of zero temperature. The parameter ξ_{coh}/r_0 contained essential information for our consideration. The factor $(\xi_{coh}/r_0)^2$ reduces to the expression $x(\xi_{coh}/a)^2$, which has a simple physical meaning: it is the total electric charge of $(\xi_{coh}/a)^2$ number of plaquettes, each having a charge x . Conversely, the parameter ξ_{coh}/r_0 describes the average spatial overlapping degree of two or more holes by one NR. If $\xi_{coh}/r_0 > 1$ then all NRs will be in close contact with each other, thus providing bulk superconductivity in the percolation regime.

In Table I, we outline the doping x dependencies for the function $(\xi_{coh}/r_0)^2$ for fixed experimental values $\xi_{coh} = 10\text{\AA}$ (the minimal size of the NR) and $\xi_{coh} \approx 13\text{\AA}$ taken from Ref. [11] and Ref. [12], respectively, and for the function ξ_{coh} , which fits $(\xi_{coh}/r_0)^2$ to $(10\text{\AA}/r_0)^2$ at $x = 0.28$ and for $x = 0.05$ provides $(\xi_{coh}/r_0)^2 \approx 1.0$. Numerical values for the ξ_{coh}/r_0 ratio are also shown in the table.

As is seen in Table I, the charges $(10\text{\AA}/r_0)^2$, $(13\text{\AA}/r_0)^2$, and $(\xi_{coh}/r_0)^2$ vary continuously with the doping x . This is not surprising because they are functions of $r_0(x)$ and $\xi_{coh}(x)$. From the analysis at the first critical doping, $x_{c1} = 0.05$, it follows that the charge $(\xi_{coh}/r_0)^2$ of the visualized NR in Ref. [11] equals +1. Thus, it corresponds to the charge of a single hole. We note that at the critical doping $x_{c1} = 0.05$, the percolation parameter is given by $\xi_{coh}/r_0 = 1.0$. This means the whole sample is entirely covered with mini areas $\xi_{coh}^2 = r_0^2$ contacting each other. It is unexpected that at the second critical doping, $x_{c2} = 0.28$, the charge of the visualized NR takes the value +2. This implies that at $\xi_{coh}^2 = 2r_0^2$, one has a

| x | $(10\text{\AA}/r_0)^2$ | $(13\text{\AA}/r_0)^2$ | $\xi_{coh}(\text{\AA})$ | $(\xi_{coh}/r_0)^2$ | ξ_{coh}/r_0 | N_{ob} |
|------|------------------------|------------------------|-------------------------|---------------------|-----------------|----------|
| 0.28 | 1.939 | 3.277 | 10 | 1.939 | 1.393 | ~ 1 |
| 0.22 | 1.524 | 2.575 | 10 | 1.524 | 1.235 | ~ 2 |
| 0.16 | 1.108 | 1.873 | 11 | 1.341 | 1.158 | ~ 3 |
| 0.14 | 0.969 | 1.638 | 12 | 1.396 | 1.182 | ~ 3 |
| 0.10 | 0.693 | 1.170 | 13 | 1.170 | 1.082 | ~ 6 |
| 0.05 | 0.346 | 0.585 | 17 | 1.000 | 1.000 | |
| 0.04 | 0.277 | 0.468 | 18 | 0.897 | 0.947 | |
| 0.02 | 0.139 | 0.234 | 20 | 0.554 | 0.744 | |

TABLE 1. The doping x dependencies of NR charges. The doping x dependencies for $(10\text{\AA}/r_0)^2$, $(13\text{\AA}/r_0)^2$ at fixed $\xi_{coh} = 10\text{\AA}$ and $\xi_{coh} = 13\text{\AA}$, respectively, for the coherent length ξ_{coh} , the charge $(\xi_{coh}/r_0)^2$ and the percolation parameter ξ_{coh}/r_0 at this ξ_{coh} are presented. The values for the number N_{ob} of bosons surrounding every fermion are shown in the last column.

pair of holes inside the NR and, as a result, the superconductivity disappears completely. For $x_{c2} = 0.28$, we have $\xi_{coh}/r_0 > 1.0$, so that the charge conductivity of the fermions still remains. As we presently understand, the normal state charge conductivity is provided only by percolated fermions-holes and at temperature $T = 0$ from x_{c2} doping, while at $T \neq 0$ by these fermions above the PG temperature boundary, for temperatures between T_c and PG boundary there exists (fermion-boson) MIC.

Notice, that there are no particles in the nature with a fractional charge, except quasi-particles, which can be produced by many-body correlations like in the fractional quantum Hall effect [21]. Hence, the problem having an extra fractional charge present inside the NR has yet to be solved. We are reminded in [11, 12] that the PG-visualized NRs constitute the bulk HTS phase below the critical temperature T_c , and therefore, they are a precursor for that phase. This undoubtedly implies that the NRs represent bosons at least. At $x_{c1} = 0.05$ one has the charge $(\xi_{coh}/r_0)^2 = 1$, so that one may surmise that the NR simply represents a boson localized in a square box ξ_{coh}^2 .

For $x > 0.05$, the charge $(\xi_{coh}/r_0)^2$ has fractional part in addition to that of the +1 (boson) part. We assign the former as the fractional part of a fermion charge. Thus, the total charge $(\xi_{coh}/r_0)^2$ of the NR includes a charge +1 for the boson and the fractional charge for the fermion. However, as mentioned above, the fractional charge cannot exist. Therefore, we take the number N_{ob} of NRs to be equal to the inverse value of the fractional part to form a charge of +1 for the fermion. As a result, we obtain one fermion surrounded by N_{ob} bosons. The values of N_{ob} are outlined in the last column of the Table 1.

The NRs introduced in such a manner allow one to understand clearly the fermion evolution over the following range $0.05 \leq x \leq 0.28$ of doping and to explain the origin of the second critical doping level, $x_{c2} = 0.28$. It is clear, that as x increases, the number of fermions increases inside the HTS phase. This means, that at x_{c2} , when the number of fermions becomes equal to the number of bosons, one has a breaking of the boson percolation lines, and, thus the HTS disappears.

The schematic single hole bosonic phase diagram for $Bi_2Sr_2CaCu_2O_{8+\delta}$ is depicted in the Fig. 4. The colored zones indicate the percentage of the sample that is gapped at a given temperature and doping. The solid lines correspond to the following observed

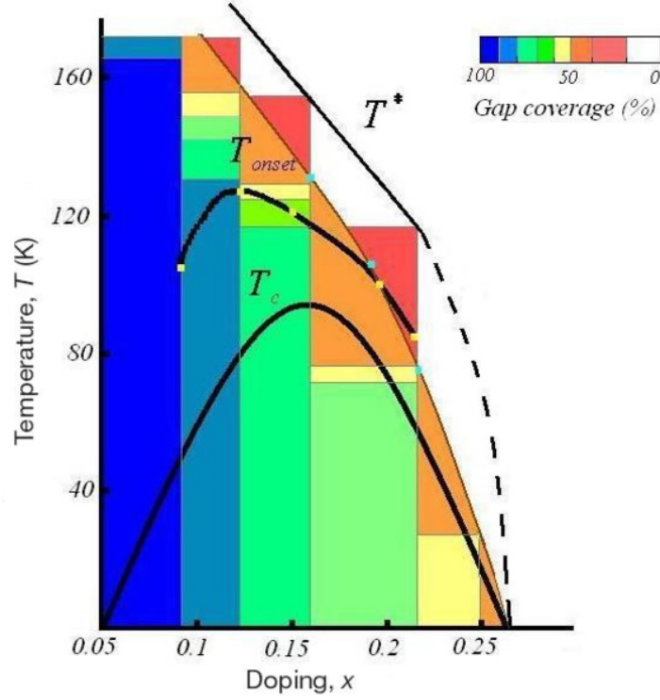


FIG. 4. Schematic single hole bosonic phase diagram for $Bi_2Sr_2CaCu_2O_{8+\delta}$

temperatures: PG boundary T^* and onset temperature T_{onset} for the Nernst effect signals taken from Ref. [37], and the critical temperature T_c from Ref. [11]. The extrapolation for the connection of T^* with the second critical doping, x_{c2} , is depicted by the dashed line. The yellow points correspond to fixed T_{onset} values from Ref. [37], and the blue points represent the temperature data for 50% of the gapped area in the sample from Ref. [11] measured at fixed dopings. The thin brown solid line fits the blue points. The percentage for the gapped doping is calculated using the equation $(1 - 1/(N_{ob} + 1)) \cdot 100\%$ under the assumption that the NRs overlap each other. It is remarkable that the T_{onset} line is substantially located in the brown zones, which means there is no bulk bosonic property above these zones.

The important qualitative issue, which is a result of the experiment performed in [11], will now be discussed. The random positions in real space for the observed pairs totally exclude any mechanism for pair formation. Since they are occasionally positioned in this space, coherent excitations (phonons, magnons or other quasi-particles), which create pairs, are problematic if the system is homogenous. The last observation deduced from the Gomes *et al.* paper, is the fundamental argument for the justification of the single hole nature of the cuprate physics.

Summarizing the physics of the above sections, we are at the stage to formulate the main positions of our Coulomb single boson and single fermion two liquid model. 1. The doping charges, in the form of individual NRs, are embedded in the insulating parent compound of HTS copper oxides. 2. Before the first critical doping level x_{c1} with NR size $\xi_{coh} = 17\text{\AA}$, they are not percolated single bosons. 3. The origin of single bosons is in the anyon bosonization of 2D fermions. 4. At the first critical doping level x_{c1} , percolation of single boson NRs and thus HTS appears; there also appears from x_{c1} doping single fermions, but up to second critical doping x_{c2} their NRs do not percolate, thus, single fermions between x_{c1} and x_{c2} are insulating. 5. The value $x_{c1} = 0.05$ is universal for all copper oxide HTSs, since percolating single boson NRs cover 50% of a 2D sample area (like connecting squares

in a chessboard); the same situation takes place with NRs for fermions at x_{c2} . 6. The normal phase charge conductivity appears from x_{c2} at $T = 0$ or above the PG temperature boundary $T = T^*$, where the percolation of single fermions appears, while for temperatures between T_c and T^* , there exists (fermion-boson) MIC. 7. The spatially rare charge density object, single boson, with NR size between $\xi_{coh} = 17\text{\AA}$ and $\xi_{coh} = 10\text{\AA}$, which correspond to x_{c1} and x_{c2} dopings, has zero total but fluctuating spin inside the NR (this rareness also leads to a fluctuating charge inside the NR). 8. Increasing the bosons' spin fluctuations with doping or temperature results in a transition of bosons into fermions, which occurs at PG T^* or at x_{c2} . 9. At zero external magnetic field, the HTS is result of the Bose-Einstein condensate for single bosons. 10. At high external magnetic fields, the PG insulating ground state is a result of the plasmon gas of these bosons.

7. Hidden magnetic order and electronic nematicity experiments

First observed in $YBa_2Cu_3O_{6+x}$ (Y123), using polarized elastic neutron diffraction [13], the hidden magnetic order has subsequently been found in three other copper oxide families: $HgBa_2CuO_{4+\delta}$ (Hg1201) [38,39], $La_{2-x}Sr_xCuO_4$ (La214) [40] and $Bi_2Sr_2CaCu_2O_{8+\delta}$ (Bi2212) [41] (see for references also [42]). Since the size of detection was a few structural cells, it was called the intra-unit-cell (IUC) hidden magnetic order.

This interesting experiment has revealed the existence of IUC objects in the PG phase with fluctuating spin components inside, which exactly cancel each other, so that the total spin of the every object was zero. Despite the authors of Ref. [13] having interpreted the physics of both, total and intra, spins either by invoking of a pair of oppositely flowing intra structural cell charge loop-currents or of staggered spins in the same cell, the role of these objects in the physics of copper oxides was not understood [43].

This role becomes unambiguously clear, if we connect these objects with the visualization of NR's which exhibit an energy gap in the STM experiment [11]. Since, as NR's, they exist in the PG region and disappear at the PG temperature boundary T^* [13]. There is no doubt that their evolution with temperature will be the same as for NRs. While their evolution with doping (see Refs. [13, 38, 39]) qualitatively coincides with that of NR's, described in [10]. However, minimal size NR's are single bosons, therefore, the IUC hidden magnetic order objects are also single bosons and PG and HTS pairs.

On the other hand, the spatially intra rare charge density of each single boson allows one to understand the nature of the intra unit cell electronic nematicity (the dynamic charge fluctuations) which were recently observed in the STM experiment [14]. The strong ferrielectric crystal field of the parent compound forms an atomic scale charge distribution within an individual NR. It is interesting that this distribution consists of fractional charges, since the charge of NR is one, attached to each atom of parent cuprate, which can be seen in the experiment.

The evolution of the dynamic charge fluctuations with doping resembles that of the IUC hidden magnetic order [7] (Ref. [7] contains a very thorough up-to-date list of references on the subject of IUC spin and charge fluctuations).

8. MIC and insulating ground state

The experimental investigation of lightly underdoped copper oxides, $La_{2-x}Sr_xCuO_4$, La_2CuO_4 , $YBa_2Cu_3O_x$, has revealed the MIC behavior in the $a - b$ plane resistivity at zero magnetic field [1], when the resistivity decreased with lowering temperature and then began to increase from its minimum value.

A similar MIC behavior for this resistivity has been observed for higher (up to critical) doping levels in several classes of HTS cuprates [2]: $La_{2-x}Sr_xCuO_4$, electron doped $Pr_{2-x}Ce_xCuO_4$, $Bi_2Sr_{2-x}La_xCuO_{6+\delta}$, under strong magnetic fields (up to 60 T), when the HTS was suppressed. The temperature-MIC boundary in the temperature-doping phase diagram resembles the temperature-PG boundary dependence.

The insulating ground state is intrinsic and robust, and therefore, belongs to the class which is fundamental for understanding the whole of HTS cuprates-based physics. As we pointed out in the introduction, it may be a result of a gas of single bosons, or more precisely, of a gas of 2D plasmons from singly-charged bosons, which is insulating, when the Bose-Einstein condensate of these bosons vanishes under a strong magnetic field or at lowering and tending of doping to the first critical value.

9. Fermi pockets and stripe phases

Fermi pockets and stripe phases belong to a very relevant and highly controversial subject of the PG cuprate physics. The experimental situation is that Fermi pockets, except for quantum oscillation experiments performed in a strong magnetic field [9], have been detected in an ARPES experiment once in an underdoped PG region with doping $x = 0.1$ and zero magnetic field above T_c in $YBa_2Cu_3O_{6+x}$ (see Fig.2 of Ref. [43]). However, stripe phases (density waves) are not observed in all copper oxides [8]. Nevertheless, Fermi pockets and stripe phases are well established in cuprate-based physics and, probably, the comprehensive description of their state-of-art and critical analysis is made in the second review of Ref. [8].

There is a widely accepted belief that there is a relationship between these two objects and furthermore, through Fermi surface reconstruction, stripe phases induce the formation of Fermi pockets (see reviews [8,43] and references therein). We consider both these objects as experimentally independent ones and try to understand their appearance within our Coulomb two liquid model.

Fermi pockets, as constituents of a Fermi surface, are a signature of fermion statistics. A manifestation of fermions in a parent compound's Brillouin zone starts at low dopings in the form of Fermi arcs [7]. Then, upon evolution with doping, it acquires Fermi pockets, and, finally, after optimal doping, it becomes circle-like, as for a homogenous Fermi gas.

The authors of quantum oscillation experiments, through the measurement of magnetoresistance oscillations at high magnetic fields in the underdome region of the temperature-doping phase diagram, have observed the Fermi liquid-like behavior of conducting quasi-particles and that measured Fermi surface had a form of Fermi pockets. This effect was found for dopings up to the optimal level for the YBCO family of cuprates (see second review of Ref. [8] for references, where there is an indication that the quantum oscillations have also been found in an electron doped cuprate). Unfortunately, this observation, under the mentioned conditions, has not been reproduced by the ARPES experiment.

However, as we pointed out in Sec. 8, for $x = 0.1$ doping and temperatures between T_c and the PG boundary T^* the system is close to the insulating state. Therefore, the Fermi pockets, found by the ARPES experiment, belong to fermions in the insulating state. This finding confirms position 4 of our Coulomb two liquid model (see end of Sec. 6), i.e. that holes-fermions between two critical dopings x_{c1} and x_{c2} are insulating, because of absence of percolation between their NRs. In our description, two limiting values for the Fermi pocket wave vector are approximately determined as $k_{F1} \approx 2\pi/\xi_{coh}(x_{c2})$ and $k_{F2} \approx 2\pi/\xi_{coh}(x)$, where x is a current doping.

As it was shown in Fig. 8 of Ref. [44], in which the schematic evolution of the nematic and stripe charge order phases with doping in underdoped cuprates is displayed, a nematic

charge order, with violation of the system rotational symmetry and small spatial size of this order, dominates at initial dopings of the HTS dome phase diagram. As we discussed in Sec. 7, the size of the nematic order coincides with the NR of single bosons. Therefore, the origin of this order is in the dynamical charge fluctuations inside the mentioned NR.

As is also seen from Fig. 8 of Ref. [44], the stripe phase appears for dopings close to the optimal (critical) one, where NRs for single fermions dominate the NRs for single bosons. This argument allows us to propose that the static charge order (stripe), which violates the parent lattice translational symmetry, is the result of insulating single fermions.

10. Why ground state of YBCO is Fermi liquid oscillating and of Bi-2212 is insulating?

As was mentioned in the previous section, the quantum oscillation experiment clearly indicates that the ground state of copper oxides from the YBCO family, in a strong magnetic field, is Fermi liquid-like, as is the case for conventional superconductors. Conversely, these copper oxides are absent in the list of materials (see section 8 or Ref. [2]), whose ground state is insulating in the same magnetic field. Does this mean that these quantum oscillating and insulating phenomena are the outcome of a single description for cuprates?

It seems, the answer to this question is “no” and it is in the following. The strong magnetic field “excites” a single boson from its ground state, so it occupies the first excited level of the system’s fermion state. Physically, a NR with a single boson occupation transits into a NR with a single fermion one. Therefore, all new formed single fermion NRs may provide percolation paths for the manifestation of the bulk Fermi liquid property, if the value for a critical doping x_c is low, as, for instance, the $x_c = 0.19$ for YBCO HTS compounds. This is the reason why holes-fermions in the quantum oscillation experiment are conducting. However, originally, without a strong magnetic field, they existed in an insulating state.

However, if the value for a critical doping x_c is large, as the $x_c = x_{c2}$ for *Bi-2212*, i.e., $Bi_2Sr_2CaCu_2O_{8+\delta}$ HTS compound, then single fermion NRs may not provide percolation paths for a bulk Fermi liquid conductor and the ground state of *Bi-2212* material in a strong magnetic field is insulating (see Ref. [45]).

11. Non-Fermi liquid heat conductivity and entropy

The puzzling side of the PG normal phase is that in this region some experimental data clearly demonstrate a failure of the Landau Fermi liquid theory (LFLT), which is the basis of the theory for normal metals. Hill et al. [3] reported that the heat conductivity of the electron doped copper-oxide $Pr_{2-x}Ce_xCuO_4$ measured at low temperature (low-T) deviated from the value predicted by the LFLT, i.e., as the temperature decreases, the temperature dependence of the heat conductivity (κ) changes from a normal linear $\kappa \sim T$ behavior into an anomalous $T^{3.6}$ one, which was described by the “downturn” behavior of the heat conductivity. They also reported another important non-Fermi liquid behavior: the Lorentz ratio of the Wiedemann – Franz law (WFL) in the region of the linear T-dependence of κ was significantly larger (1.7 times) than Sommerfeld’s value. These violations were also observed in the $Bi_{2+x}Sr_{2-x}CuO_{6+\delta}$ copper-oxide in the vicinity of the metal-insulator-crossover by Proust *et al.* [4].

The normal state electronic specific heat, c , for superconductors $YBa_2Cu_3O_{6+x}$ and $La_{2-x}Sr_xCuO_4$ above the high- T_c transition temperature T_c was experimentally investigated in [5] and [6], respectively. Due to existence of high- T_c superconductivity, it is impossible to extract information on the low- T dependence of the normal state c . On the other hand, Loram *et al.* [5] showed the T -dependence of the entropy (\mathcal{S}) $\mathcal{S} \sim T^i$ with $i > 1$ for the

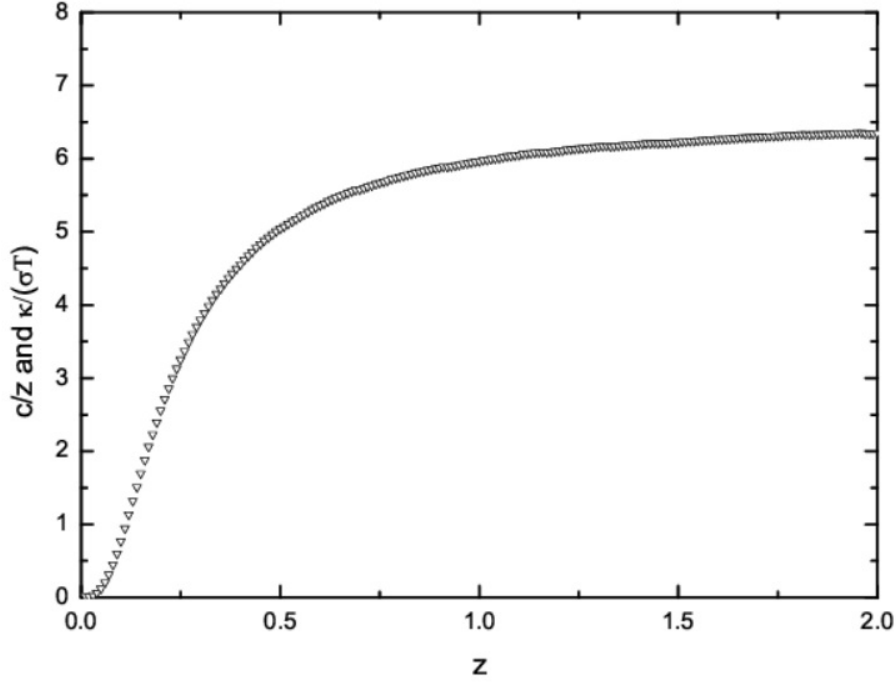


FIG. 5. The specific heat c/z and WFL $\kappa/(\sigma T)$ as function of z , where z is linearly proportional to temperature.

underdoped (insulating) material, which was driven from the measured electronic specific heat, ignoring the superconducting effects, while for the optimal doping compound, $\mathcal{S} \sim T$ was measured.

In Ref. [46], we tried to understand these non-Fermi liquid properties of the low- T heat conductivity, the specific heat and entropy of copper-oxides within a Coulomb two-liquid model, consisting of single boson and fermion holes.

In Fig. 5 we have plotted WFL and specific heat as a function of temperature for compounds investigated experimentally in Refs. [3] and [5,6]. Experiment [3] shows $\kappa \sim T^{3.6}$ for normal state quasiparticles, while our dependence is $\kappa \sim T^4$ and connected with the specific heat dependence $c_1 \sim T^4$ for the Coulomb Bose gas (single bosons).

For the Lorentz ratio of the WFL we have derived in Ref. [46] the formula:

$$L = L_0 \left[\frac{3.106}{t^{1/3}} \left(1 - \frac{t}{t_c} \right) + \frac{t}{t_c} \right], \quad (23)$$

where t and $t_c \approx 0.19$ (see [30]) are dopings, $L_0 = (\pi^2/3)(k_B/e)^2$ is the Fermi liquid Sommerfeld's value of the Lorentz ratio and the first term in square brackets originated from the single boson WFL $\kappa/(\sigma T) = 3.106 \cdot L_0/t^{1/3}$. In Fig. 6, we displayed L/L_0 as function of t in comparison with its values measured for different cuprates. The good agreement for L/L_0 with experimental data is obvious.

In Ref. [46], we also obtained the expression of the normal state entropy \mathcal{S} :

$$\mathcal{S} = \frac{c_1}{4} \left(1 - \frac{T}{T^*} \right) + c_F \frac{T}{T^*}, \quad (24)$$

where, c_F is the heat capacity for a gas of fermions and T^* is the PG boundary temperature. The entropy, as function of temperature at various dopings t , is depicted in Fig. 7. Comparing the calculated dependencies for \mathcal{S} with the experimental ones from Ref. [5], we

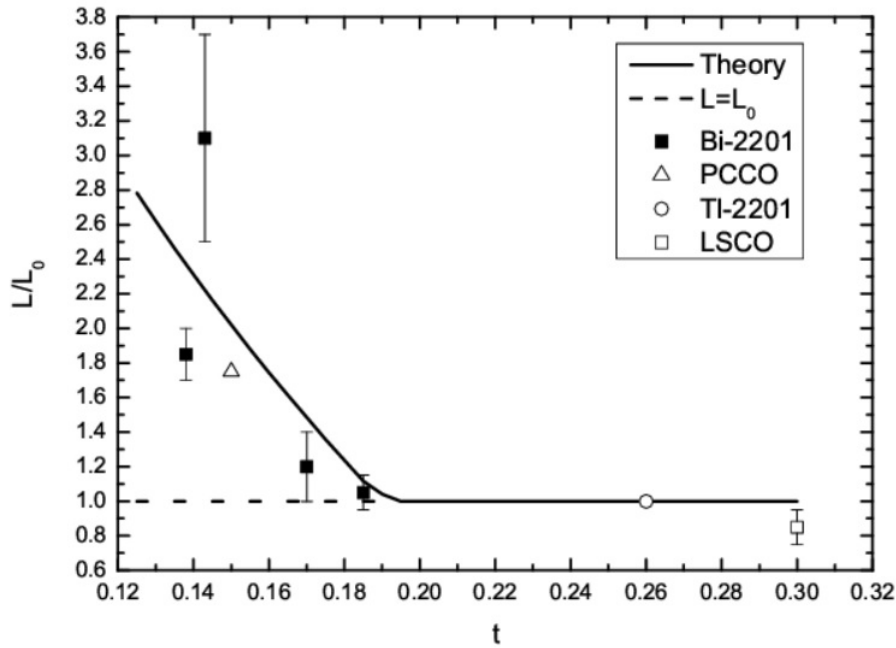


FIG. 6. The Lorentz ratio L/L_0 (Eq. (23)) vs. t (values for $t \geq 1$ are added artificially). Observed dots are from Ref. [4]

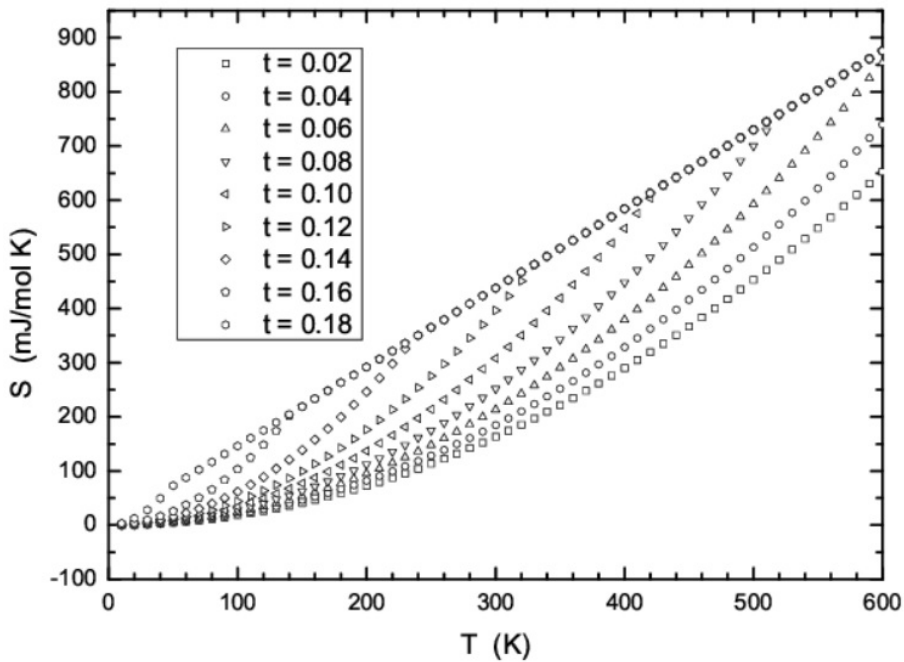


FIG. 7. The entropy \mathcal{S} (Eq. (24)) vs. T at various t (values of \mathcal{S} behind the crossing of linear and nonlinear parts of \mathcal{S} are added artificially)

see again the good agreement. As shown in [46], the nonlinear T dependence of the entropy \mathcal{S} at small temperatures is related to the insulating ground state.

12. Conclusion

In summary, we have formulated the Coulomb single boson single fermion two liquid model positions for HTS copper oxides: 1. The doping charges, in the form of individual NRs, are embedded in the insulating parent compound of HTS copper oxides. 2. Before the first critical doping x_{c1} with NR size $\xi_{coh} = 17\text{\AA}$, they are not percolated single bosons. 3. The origin of single bosons is in the anyon bosonization of 2D fermions. 4. At the first critical doping level, x_{c1} , the percolation of single boson NRs and thus HTS appears; there appear also from x_{c1} doping single fermions, but up to second critical doping level, x_{c2} , their NRs do not percolate, thus single fermions between x_{c1} and x_{c2} are insulating. 5. The value $x_{c1} = 0.05$ is universal for all copper oxide HTSs, since percolating single boson NRs cover 50% of the 2D sample area (like connecting squares in a chessboard); the same situation takes place with NRs for fermions at x_{c2} . 6. The normal phase charge conductivity appears from x_{c2} at $T = 0$ or above PG temperature boundary $T = T^*$, where the percolation of single fermions appears, while for temperatures between T_c and T^* , there exists (fermion-boson) MIC. 7. The spatially rare charge density object, single boson, with NR size between $\xi_{coh} = 17\text{\AA}$ and $\xi_{coh} = 10\text{\AA}$, which correspond to x_{c1} and x_{c2} dopings, has zero total but fluctuating inside of NR spin (this rareness leads also to fluctuating charge inside the NR). 8. The increase of boson spin fluctuations with doping or temperature results in a transition of bosons into fermions, which occurs at PG T^* or at x_{c2} . 9. At zero external magnetic field, the HTS is a result of the Bose-Einstein condensate of single bosons. 10. At high external magnetic field, the PG insulating ground state is the result of a plasmon gas consisting of these bosons.

Within these positions, we have succeeded in understanding the following constituents of the doping-temperature phase diagram for hole-doped copper oxides: (i) the first and second critical doping levels are a result of the emergence and disappearance of the single hole boson percolation lines, respectively; (ii) the disappearance of the percolation lines leads to the end of PG bulk bosonic property or to the end of Nernst effect signals; (iii) the fact that the PG boundary was bound, where the single hole bosons disappear, was confirmed by Ref. [11]. Our findings are consistent with the recent observation [47] of the superconducting phase which consisted of an array of nanoclusters embedded in an insulating matrix and of the percolative transition to this phase from the normal phase in $YBa_2Cu_3O_{6+\delta}$. A recent experiment [48] also displayed the percolative superconductor-insulator quantum phase transition in electron-doped $Pr_{2-x}Ce_xCuO_4$. Superconducting islands, introduced in insulating background, have been used to interpret the superconductor-insulator transition in $Bi_2Sr_{2-x}La_xCaCu_2O_{8+\delta}$ compound [49].

We are reminded of the possible scenario for the origin of PG phase in the copper-oxides. In Ref. [16], we pointed out that the PG boundary exactly coincides in the experiment with the structural phase transition line, where the symmetry of the sample structure changes. However, the structural phase transition induces a mechanical strain in the system. This mechanical strain changes the magnetic phase transition, existing in a system, from a second order into a first order one. However, this first order phase transition is close to the second order one. This effect is referred to in the literature as a striction. The phase transition of single bosons into fermions, discussed in Sec. 4, is possibly governed by a striction. Therefore, transition peaks in the specific heat increment are washed out in the cuprate underdoping regime [5]. On the other hand, the first order phase transition accepts the existence of a meta-stable phase. We believe that the PG phase of cuprates is a meta-stable phase of single bosons, whose effective spins are fluctuating and interacting with each

other. At the PG boundary, this interaction entirely destroys bosons, transforming them into fermions.

We predict the existence of non-percolated single bosons at low- T before the first critical doping x_{c1} in the doping-temperature phase diagram of copper-oxides, which is already seen in the experiment (see below). For these dopings, a scanning tunneling microscopy measurement may probe the same picture for minimal size NRs as for PG region, close to PG boundary. The Bose statistics of these particles may be experimentally detected by some methods described in Ref. [50]. These methods might also be applied to detect the insulating fermions inside the HTS dome, which is the main hypotheses of the present treatment.

We predict the existence of quantum oscillations in the ground state for copper oxides in a strong magnetic field with low critical doping values x_c and an insulating phase for HTS compounds having large x_c values.

Our Coulomb two liquid model also predicts there to be no Josephson and Andreev effects between the two $a - b$ planes of the underdoped HTS, belonging to two cuprates and separated by an insulating layer. It would be interesting to probe the atomic scale fractional charges in the STM experiment for electronic nematicity.

Recently, authors of Ref. [51] have reported on the emergent transition for superconducting fluctuations in the deep antiferromagnetic phase at a remarkably low critical doping level, $x_c = 0.0084$, for ruthenocuprates, $RuSr_2(R, Ce)_2Cu_2O_{10-\delta}$ with $R = Gd, Sm, Nd$. In this paper, it was claimed that those fluctuations have an intrinsic electronically-inhomogenous nature and provide new support for bosonic models of the superconducting mechanism.

In conclusion, we point out that the present paper is a substantially extended and critically revised version of our previous Ref. [52], in which we added the alternative physical insight into the background of HTS physics.

Acknowledgements

Authors B. Abdullaev and C.-H. Park acknowledge the support of the research by the National Research Foundation (NRF) Grant (NRF-2013R1A1A2065742) of the Basic Science Research Program of Korea.

References

- [1] Takagi H. et al. Systematic evolution of temperature-dependent resistivity in $La_{2-x}Sr_xCuO_4$. *Phys. Rev. Lett.*, 1992, **69**, P. 2975–2979; Keimer B. et al. Magnetic excitations in pure, lightly doped, and weakly metallic La_2CuO_4 . *Phys. Rev. B*, 1992, **46**, P. 14034; Wuyts B., Moshchalkov V. V., Bruynseraede Y. Resistivity and Hall effect of metallic oxygen-deficient $YBa_2Cu_3O_x$ films in the normal state. *Phys. Rev. B*, 1996, **53**, P. 9418; Abe Y. et al. Normal-state magnetotransport in $La_{1.905}Ba_{0.095}CuO_4$ single crystals. *Phys. Rev. B*, 1999, **59**, P. 14753.
- [2] Ando Y. et al. Logarithmic Divergence of both In-Plane and Out-of-Plane Normal-State Resistivities of Superconducting $La_{2-x}Sr_xCuO_4$ in the Zero-Temperature Limit. *Phys. Rev. Lett.*, 1995, **75**, P. 4662–4665; Boebinger G. S. et al. Insulator-to-Metal Crossover in the Normal State of $La_{2-x}Sr_xCuO_4$ Near Optimum Doping. *Phys. Rev. Lett.*, 1996, **77**, P. 5417–5420; Fournier P. et al. Insulator-Metal Crossover near Optimal Doping in $Pr_{2-x}Ce_xCuO_4$: Anomalous Normal-State Low Temperature Resistivity. *Phys. Rev. Lett.*, 1998, **81**, P. 4720–4723; S Ono S. et al. Metal-to-Insulator Crossover in the Low-Temperature Normal State of $Bi_2Sr_{2-x}La_xCuO_{6+\delta}$. *Phys. Rev. Lett.*, 2000, **85**, P. 638–641; Ando Y. et al. Supporting evidence of the unusual insulating behavior in the low-temperature normal-state resistivity of underdoped $La_{2-x}Sr_xCuO_4$. *J. Low Temp. Phys.*, 1996, **105**, P. 867–875.
- [3] Hill R. W. et al. Breakdown of Fermi-liquid theory in a copper-oxide superconductor. *Nature*, 2001, **414**, P. 711–715.
- [4] Proust C. et al. Heat transport in $Bi_{2+x}Sr_{2-x}CuO_{6+\delta}$: Departure from the Wiedemann-Franz law in the vicinity of the metal-insulator transition. *Phys. Rev. B*, 2005, **72**, P. 214511.

- [5] Loram J. W. et al. Electronic specific heat of $YBa_2Cu_3O_{6+x}$ from 1.8 to 300 K. *Phys. Rev. Lett.*, 1993, **71**, P. 1740–1743.
- [6] Loram J. W. et al. Evidence on the pseudogap and condensate from the electronic specific heat. *J. Phys. Chem. Solids*, 2001, **62**, P. 59–64.
- [7] Fujita K. et al. Simultaneous Transitions in Cuprate Momentum-Space Topology and Electronic Symmetry Breaking. *Science*, 2014, **344**, P. 612–616.
- [8] Vojta M. Lattice symmetry breaking in cuprate superconductors: stripes, nematics, and superconductivity. *Adv. Phys.*, 2009, **58**, P. 699–820; Vojta M. Stripes and electronic quasiparticles in the pseudogap state of cuprate superconductors. *Physica C*, 2012, **481**, P. 178.
- [9] Sebastian S. E., Harrison N., Lonzarich G. G. Towards resolution of the Fermi surface in underdoped high- T_c superconductors. *Rep. Prog. Phys.*, 2012, **75**, P. 102501.
- [10] Abdullaev B., Park C.-H., Musakhanov M. M. Anyon bosonization of 2D fermions and single boson phase diagram implied from experiment on visualizing pair formation in superconductor $Bi_2Sr_2CaCu_2O_{8+\delta}$. *Physica C*, 2011, **471**, P. 486–491.
- [11] Gomes K. K. et al. Visualizing pair formation on the atomic scale in the high- T_c superconductor $Bi_2Sr_2CaCu_2O_{8+\delta}$. *Nature*, 2007, **447**, P. 569–572.
- [12] Pan S. H. et al. Microscopic electronic inhomogeneity in the high- T_c superconductor $Bi_2Sr_2CaCu_2O_{8+x}$. *Nature*, 2001, **413**, P. 282–285.
- [13] Fauque B. et al. Magnetic order in the pseudogap phase of high- T_C superconductors. *Phys. Rev. Lett.*, 2006, **96**, P. 197001.
- [14] Lawler M. J. et al. Intra-unit-cell electronic nematicity of the high- T_c copper-oxide pseudogap states. *Nature*, 2010, **466**, P. 347–351.
- [15] Abdullaev B., Roessler U., Musakhanov M. An analytic approach to the ground state energy of charged anyon gases. *Phys. Rev. B*, 2007, **76**, P. 075403(1-7).
- [16] Abdullaev B. *Implicit Anyon or Single Particle Boson Mechanism of HTCS and Pseudogap Regime*. In Trends in Boson Research, edit. by A. V. Ling. N. Y.: Nova Science Publisher Inc., 2006, p. 139–161.
- [17] B. Abdullaev B., Park C.-H. Bosonization of 2D Fermions due to Spin and Statistical Magnetic Field Coupling and Possible Nature of Superconductivity and Pseudogap Phases Below E_g . *J. Korean Phys. Soc.*, 2006, **49**, P. S642–S646; arxiv:cond-mat/0404668.
- [18] Leinaas J. M., Myrheim J. On the Theory of Identical Particles. *Nuovo Cimento Soc. Ital. Fis. B*, 1977, **37**, P. 1–23.
- [19] Wilczek F. Magnetic Flux, Angular Momentum, and Statistics. *Phys. Rev. Lett.*, 1982, **48**, P. 1144–1147.
- [20] Dunne G. et al. Exact multi-anyon wave functions in a magnetic field. *Nucl. Phys. B*, 1992, **370**, P. 601–635.
- [21] Laughlin R. B. in The Quantum Hall Effect, Edited by R. E. Prange and S. M. Girvin. New York, Springer-Verlag, 1987.
- [22] Wu Y. -S. Multiparticle Quantum Mechanics Obeying Fractional Statistics. *Phys. Rev. Lett.*, 1984, **53**, P. 111–115. Erratum *ibid*, 1984, **53**, P. 1028.
- [23] Comtet A., McCabe J., Ouvry S. Perturbative equation of state for a gas of anyons. *Phys. Lett. B*, 1991, **260**, P. 372–376.
- [24] Bonsal L., Maradudin A. A. Some static and dynamical properties of a two-dimensional Wigner crystal. *Phys. Rev. B*, 1977, **15**, P. 1959.
- [25] Rajagopal A. K., Kimball J. C., Correlations in a two-dimensional electron system. *Phys. Rev. B*, 1977, **15**, P. 2819.
- [26] Tanatar B., Ceperley D. M. Ground state of the two-dimensional electron gas. *Phys. Rev. B*, 1989, **39**, P. 5005.
- [27] De Palo S., Conti S., Moroni S. Monte Carlo simulations of two-dimensional charged bosons. *Phys. Rev. B*, 2004, **69**, P. 035109.
- [28] Attacalite C. et al. Correlation Energy and Spin Polarization in the 2D Electron Gas. *Phys. Rev. Lett.*, 2002, **88**, P. 256601; Erratum *ibid*, 2003, **91**, P. 109902.
- [29] Landau L. D., Lifshitz E. M. *Quantum Mechanics, Non-relativistic Theory*. Oxford, Pergamon Press, 1977, § 65.
- [30] Tallon J. L., Loram J. W. The doping dependence of T^* what is the real high- T_c phase diagram? *Physica C*, 2001, **349**, P. 53–68.
- [31] Onose Y. et al. Charge dynamics in underdoped $Nd_{2-x}Ce_xCuO_4$: Pseudogap and related phenomena. *Phys. Rev. B*, 2004, **69**, P. 024504.

- [32] A. Zimmers et al. Infrared properties of electron-doped cuprates: Tracking normal-state gaps and quantum critical behavior in $Pr_{2-x}Ce_xCuO_4$. *Europhys. Lett.*, 2005, **70**, P. 225.
- [33] Zaanen J. Superconductivity: Why the temperature is high. *Nature*, 2004, **430**, P. 512–513.
- [34] Uemura Y. J. et al. Universal Correlations between T_c and n/m (Carrier Density over Effective Mass) in High- T_c Cuprate Superconductors. *Phys. Rev. Lett.*, 1989, **62**, P. 2317–2320.
- [35] Uemura Y. J. et al. Basic similarities among cuprate, bismuthate, organic, Chevrel-phase, and heavy-fermion superconductors shown by penetration-depth measurements. *Phys. Rev. Lett.*, 1991, **66**, P. 2665–2669.
- [36] Kastner M. A., Birgeneau R. J., Shirane G., Endoh Y. Magnetic, transport, and optical properties of monolayer copper oxides. *Rev. Mod. Phys.*, 1998, **70**, P. 897–928.
- [37] Wang Y., Li L., Ong N. P., Nernst effect in high- T_c superconductors. *Phys. Rev. B*, 2006, **73**, 024510.
- [38] Li Y et al. Unusual magnetic order in the pseudogap region of the superconductor $HgBa_2CuO_{4+\delta}$. *Nature*, 2008, **455**, P. 372.
- [39] Li Y et al. Magnetic order in the pseudogap phase of $HgBa_2CuO_{4+\delta}$ studied by spin-polarized neutron diffraction. *Phys. Rev. B*, 2011, **84**, P. 224508.
- [40] V. Baledent V. et al. Two-Dimensional Orbital-Like Magnetic Order in the High-Temperature $La_{2x}Sr_xCuO_4$ Superconductor. *Phys. Rev. Lett.*, 2010, **105**, P. 027004.
- [41] De Almeida-Didry S. et al. Evidence for intra-unit-cell magnetic order in $Bi_2Sr_2CaCu_2O_{8+\delta}$. *Phys. Rev. B*, 2012, **86**, P. 020504.
- [42] Mangin-Thro L. et al. Characterization of the intra-unit-cell magnetic order in $Bi_2Sr_2CaCu_2O_{8+\delta}$. *Phys. Rev. B*, 2014, **89**, P. 094523.
- [43] Norman M. Fermi-surface reconstruction and the origin of high-temperature superconductivity. *Physics*, 2010, **3**, P. 86 (6 pages).
- [44] Caprara S. et al. Signatures of nematic quantum critical fluctuations in the Raman spectra of lightly doped cuprates. *Phys. Rev. B*, 2015, **91**, P. 205115.
- [45] Zavaritsky V. N. et al. Giant normal state magnetoresistances of $Bi_2Sr_2CaCu_2O_{8+\delta}$. *EPJ B*, 2004, **42**, P. 367–371.
- [46] Abdullaev B., Park C.-H., Park K.-S., Observed Non-Fermi Liquid Heat Transport and Entropy of Pseudogap Quasi-Particles as Possible Manifestations of Single Particle Bosons. // arxiv: cond-mat/0703290, 2007, 5 pages.
- [47] Gavrilkin S. Yu. et al. Percolative nature of the transition from 60 to 90 K-phase in $YBa_2Cu_3O_{6+\delta}$. *Physica C*, 2010, **470**, P. S996–S997.
- [48] Zeng S. W. et al. Two-dimensional superconductor-insulator quantum phase transitions in an electron-doped cuprate. *Phys. Rev. B*, 2015, **92**, P. 020503(R).
- [49] Oh S. et al. Doping Controlled Superconductor-Insulator Transition in $Bi_2Sr_{2-x}La_xCaCu_2O_{8+\delta}$. *Phys. Rev. Lett.*, 2006, **96**, P. 107003.
- [50] Stern A. Anyons and the quantum Hall effect – A pedagogical review. *Ann. Phys.*, 2008, **323**, P. 204.
- [51] McLaughlin A. C., Atfield J. P. Emergent Transition for Superconducting Fluctuations in Antiferromagnetic Ruthenocuprates. *Phys. Rev. B*, 2014, **90**, P. R220509.
- [52] Abdullaev B. Anyon Bosonized 2D Fermions or a Single Boson Physics of Cuprates: Experimental Evidences. In Low Dimensional Functional Materials, NATO Science for Peace and Security Series B: Physics and Biophysics 2013. Netherlands, Springer, 2013, P. 251-268.